JOURNAL OF AIRCRAFT
Vol. 45, No. 5, September–October 2008

Multiple Discipline Optimization and Aerodynamic Off-Design Analysis of Supersonic Transport Aircraft

U. Herrmann*
DLR, German Aerospace Center, D-38108 Braunschweig, Germany

DOI: 10.2514/1.32673

The multidiscipline optimization of a supersonic aircraft for longer mission range is described. A multidisciplinary analysis suite is developed based on high-fidelity modules for aerodynamics and structural mechanics at cruise and is completed by empirical modules covering other disciplines and flight regimes. This analysis suite describes the complete flight mission of a generic supersonic transport aircraft and is coupled to a global optimizer driving the global variables of the aircraft wing. Several multiple discipline optimizations are conducted covering the design space. Configurations cruising longer missions are obtained. The aerodynamic off-design characteristics of such an optimized aircraft configuration are analyzed using a Reynolds averaged Navier–Stokes method. Results for low-speed and transonic operation conditions are used to assess the prediction capabilities of the empirical models used in the mission simulation of the multidiscipline optimization process.

Nomenclature

a	=	speed of sound, m/s
a/c	=	aircraft
C	=	chord of the wing cross section
C_p	=	pressure coefficient
D	=	drag
L	=	lift
M	=	Mach number; $M = V/a$
R	=	range
S	=	local span of the wing trapezoid
V	=	cruise speed, m/s
Φ	=	wing leading edge sweep angle

I. Introduction

CURRENTLY the air travel market growing again after its abrupt decline in 2001. Part of this expanding market is asking for reduced travel times, especially for long-range connections. Beyond increasing efficiency regarding airport logistics, this also triggers a request for high-speed air transport.

Because of increasing economic and environmental constraints posed for any new aircraft (a/c) it is believed that a lower supersonic cruise Mach number (below $M = 2$) might improve the performance of a supersonic a/c and, by that, also reduce its environmental impact.

Within the Airbus Association of European Research Establishment pilot project Cruise Speed Impact on Supersonic Aircraft Planform (CISAP) [1], partners develop a common multidiscipline analysis suite (MDA). This MDA [2] combines high-fidelity modules for structural mechanics (FEM) and cruise aerodynamics (Euler CFD) and is closed using empirical models for off-design aerodynamics as well as flight mechanics and propulsion. This MDA is combined with partners own flow solvers and the NASTRAN FEM solver in an individual manner to construct multidiscipline optimization (MDO) processes. Current developments expand the applicability of this MDA also toward smaller supersonic transport configurations [3,4].

Received 7 June 2007; revision received 21 March 2008; accepted for publication 30 March 2008.

*Principal Scientist, Transport Aircraft Branch, Institute of Aerodynamics and Flow Technology, Lilienthalplatz 7; Ulrich.Herrmann@DLR.de.

Conceptual design methods define the datum configurations for two lower cruise Mach numbers [5] of 1.3 and 1.6. These configurations are to be improved through the multidiscipline (MD) optimizations to be reported. Furthermore a reference concept designed for cruise at $M = 2$ is given. All a/c have several common features: identical fuselage, four engines, double trapezium wing planform, and a maximum takeoff weight (MTOW) of 340 t. Their baseline flight mission enables them to transport 250 passengers about a distance of 5500 n miles. The assumed additional performance potential due to a reduced cruise Mach number ($M = 1.3$ to $M = 2$) is measured and expressed as mission range increases in the context of this paper.

II. The DLR Multidiscipline Optimization Process

The common MDA process within the CISAP project is adjusted to represent a generalized flight mission (see Fig. 1). For this mission, several flight phases are modeled: takeoff and climb-out, transonic cruise (A), supersonic cruise (B), and the reserves hold (C), as well as traveling to an alternate destination (D). The overall objective of this study is to obtain maximum range for an a/c with starting at a fixed MTOW. Please note that, primarily, the length of the supersonic cruise leg (B) is changing, as the other parts of the mission have smaller impact on the overall flight time and range. As most of the fuel is burned during supersonic cruise, high-fidelity tools are used to obtain a physics based modeling of this flight phase.

The layout of the used DLR MDO process is depicted in Fig. 2. The MDA (center box) is provided by the National Aerospace Laboratory (The Netherlands) and consists of modules generating the external and internal geometry, computes the configurations weight and balance, performs some engine optimization, deals with flight mechanic issues, and, finally, computes the mission range of the a/c candidate decided by the global optimizer (left box). This MDA is combined to form the DLR MDO process by adding two optimization environments (gray boxes) driving independent sets of design variables in a cascaded manner.

These two sets of design variables are displayed in Fig. 3. The figure's top half shows the geometric variables defining a double trapezium wing planform. This planform is parameterized by the indicated nine variables. At the local chords $C1$, $C2$, and $C3$, additional local twist angles and local wing thickness variables exist. The wing cross sections at these three locations are extracted from the $M = 2$ reference a/c and are not changed (except their thicknesses) throughout the optimizations.

The bottom part of Fig. 3 depicts the elements of the parametric structural layout. Their length and orientation are adjusted to fit into the wing planform defined by the previously mentioned geometric

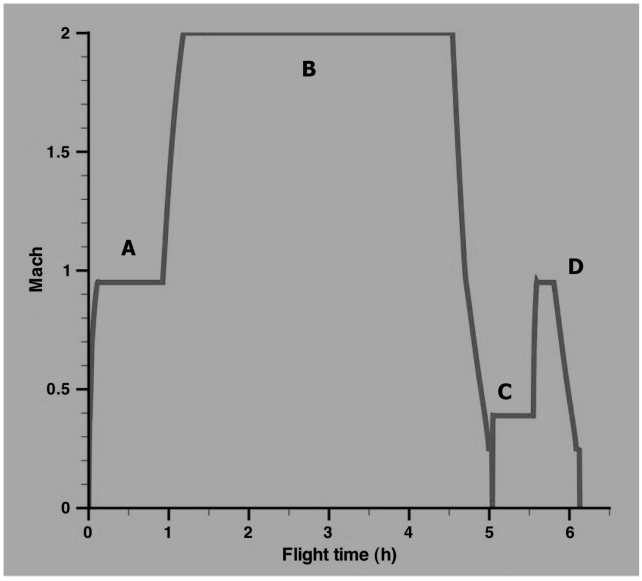

Fig. 1 Generic aircraft missions: A) sub- and transonic; B) supersonic; C) cruise leg and reserves; D) flight Mach number over flight time.

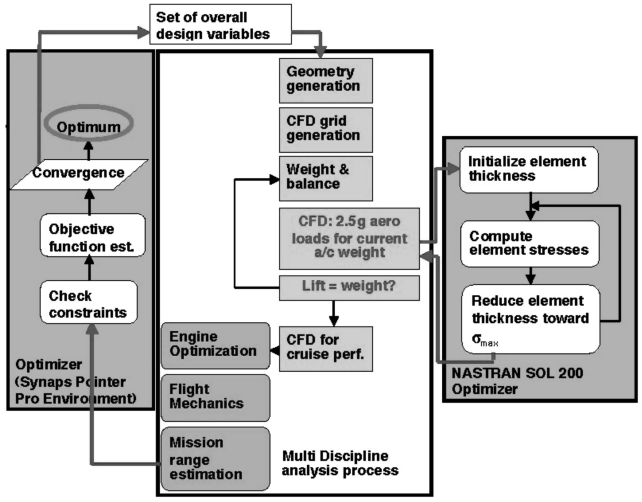

Fig. 2 Realized mixed fidelity MDO process operational at DLR.

variables. Beams and spars are indicated in bold and stringers (lumped) as thin lines. Please note the large wheel bay cut out for the main landing gear (marked black) defined by the conceptual design of this $M = 1.6$ a/c. The structural elements are grouped together to reduce the number of structural design variables (115) and to reduce the numerical effort for the NASTRAN internal optimizer.

The Synaps Pointer Pro (SPP) optimizer environment [6], left gray box in Fig. 2, drives the geometric top-level design variables and calls the MDA.

The second optimization environment, indicated by the right-hand-side gray box in Fig. 2, is the internal structural optimizer of NASTRAN [7]. It is called from within the MDA during the iterative estimation of the wing weight.

The global optimizer (provided by the SPP environment) changes the top-level wing twist, thickness, and planform variables and calls the MDA for the estimation of the range of this a/c variant. For this the first step is to perform the geometry and mesh generation (MegaCads [8]).

In the following step, simulating a 2.5 g pull-up maneuver at cruise is simulated to obtain realistic loads to dimension the elements of the wing structure.

1) The lift during this 2.5 g pull-up maneuver is guessed in the first step by the weight and balances module because the wing weight of this a/c variant is initially unknown.

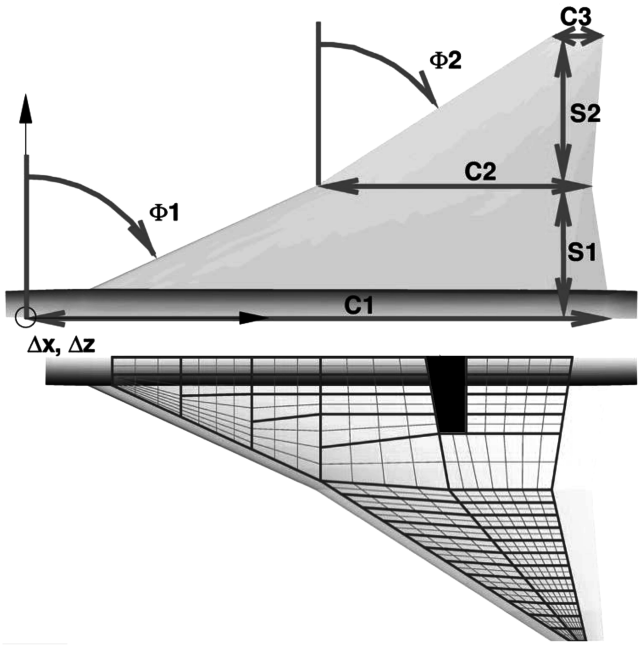

Fig. 3 Design variables of the wing geometry (top) and internal structural elements (spars and ribs in bold; lumped stringers as thin lines).

2) For this current maneuver lift, the flow is computed by the DLR FLOWer [9] code in Euler mode, and the aerodynamic load is mapped onto the wing structure.

3) The NASTRAN internal optimizer first sizes and minimizes the structural element thicknesses of the wing structure based on the aerodynamic maneuver load. The updated weight of the primary wing structure, based on the element thicknesses, is computed from this.

With this new wing weight, steps b and c are repeated until convergence is obtained (ΔC_L between two subsequent steps <0.0002, $\sim 0.2\%$ variation).

With the converged wing weight, the lift at supersonic cruise and the associated aerodynamic performance is estimated next, again using the DLR FLOWer code in Euler mode. Finally, the engine is sized, the amount of fuel (limited either by the tank volume or the MTOW) is computed, and the flight mechanic constraints are checked.

The complete mission range for the current set of geometric variables is computed by complementing the length of the supersonic cruise leg with the further mission parts. These mission parts are computed relying on empirical models. The final mission length result is reported to the SPP environment, steering the further optimization run. All posed geometric and other constraints are checked and potentially drag penalized if they are broken.

The assumed engine is a single midfan engine with variable bypass ratio and variable thermodynamic cycle. Sizing of the engines is based on a fixed runway length. Details regarding the MDA [2], the posed constraints [1], and the DLR MDO process [10] have previously been reported.

III. Multidiscipline Optimization Design Results

Numerical results of such a complex MDO process are likely to be impacted by different sources of numerical noise and cut-off errors that are always present in iterative numerical procedures. Thus, for a robust MDO process, an optimizer has to be selected that is known to be robust enough to deal with noisy objective functions. Therefore, an optimizer that does not depend on gradient information is selected (Nelder–Mead simplex [11]) from the range of available optimizers within the SPP environment.

Working with subsets of design variables minimizes the overall turn-around time of the optimization. Starting with six active design

Table 1 Optimization results for two types of optimization approach

$M = 1.6a/c$	Datum	Optimized	In %	Automated optimized	in %
Range	4968 n miles	5926 n miles	+19.3%	6017 n miles	+21.1%
Wing weight	43509 kg	25761 kg	−40.8%	24534 kg	−43.6%
Wing area	786 m^2	893 m^2	+13.4%	871 m^2	+10.8%
Target C_L	0.14	0.12	−13.6%	0.12	−13.6%
L/D	9.9	10.2	+2.9%	10.3	+4.3%

variables, several subsequent short optimization runs (with changing sets of design variables) are performed. Each run is started from the previously found optimum. This strategy is efficient because it seems to prevent the optimizer from converging too early to local minima. With this approach, a significant range improvement compared with the $M = 1.6$ datum configuration is obtained. The new a/c travels nearly 20% farther than the datum (see Table 1).

The main reason for this significant range increase lies in the computed large wing weight reduction because the optimizer drives wing planform and twisting such that the high aerodynamic load experienced at the 2.5 g pull-up maneuver is shifting inboards, and, furthermore, the structural impact of the large wheel bay cut out (see Fig. 3) on the structural integrity of the wing is reduced.

Figure 4 compares the datum and the optimized $M = 1.6$ configuration. For top and bottom surface, the pressure distributions are shown. A reduced pressure variation is obtained for the optimized configuration. The large planform change is clearly visible. The leading edge sweeps of the inner and outer wing trapezium become similar. The increasing wing chords straighten the load path such that the large wheel bay cut out (see Fig. 3) is no longer interfering with the main load path. The wing box weight therefore significantly reduces from 43.5 to 25.7 t. Twisting the outer wing shifts the aerodynamic loading inboard and supports this trend. Furthermore, the wing area increases by 13%, leading to a reduced cruise C_L and an associated small aerodynamic improvement. Further improvement is mainly due to a reduction of the local wing thicknesses enabled by the load shifting.

This optimized configurations is further assessed. The aerodynamic off-design performance is estimated by comparing high-fidelity Reynolds averaged Navier–Stokes (RANS) computation results to the empirical models predictions used within the MDO process. Results and findings of this comparison will be described in Sec. IV.

These current results (see Fig. 4), obtained by a sequence of short optimization runs featuring (manually changed) subsets of design variables, are compared with an automated approach. This automated approach uses the same number of design variables but relies on another optimizer. The alternate optimizer incorporates the feature to work on selected subsets of variables for increased efficiency. Because the advantage of sequenced short optimization runs to prevent local minima is understandable, the benefit of fully automated optimizations without user interaction is obvious.

This alternate optimizer is a subspace-searching simplex method called SubPlex [12] and, like the Nelder–Mead simplex, it is well suited for optimizing noisy objective functions. The SubPlex optimizer selects active subsets of design variables based on sensitivity analysis on demand. Furthermore, as the number of function evaluations typically increases linearly with the problem size, the SubPlex is more efficient than the simplex method for most applications because, on average, fewer variables are active. A confirmation of this behavior is obtained through pure aerodynamic optimization examples and has previously been reported [10].

Fully automated optimizations with all variables (15) are now performed using the alternate optimizer SubPlex. Only two different starting points are selected trying to verify that the SubPlex optimizer explores the full design space without converging to different local minima. This will also enable comparison of the optimization results obtained so far (using the Nelder–Mead method) to newly computed results using the SubPlex optimizer.

Figure 5 compares the a/c configuration at the start and end of such an automatically performed optimizations. The datum $M = 1.6a/c$ (designed by conceptual methods) is selected to repeat the previous MDO exercise in a single run. Although a large range increase (+11.8%) is computed, the previous optimum provided by the Nelder–Mead optimizer is not reached. This indicates that the design space seems to feature many local maxima and that the manual design approach based on a sequence of independent optimization runs with changing subsets of variables is able to prevent some of the local maxima.

To further prove this assumption, an alternate start point is selected for the second automated optimization (see Fig. 6). The wing planform design variables are tuned to come close to the $M = 2$ datum a/c, and the SubPlex optimizer converges to an optimum that slightly exceeds ($\Delta R = +21.1\%$) the previous nonautomated optimization results. This last results is added to Table 1 for comparison to the nonautomated results. These three applications obtaining different planform geometries and performance levels indicate that the design space might be complex shaped or significantly impacted by numerical noise.

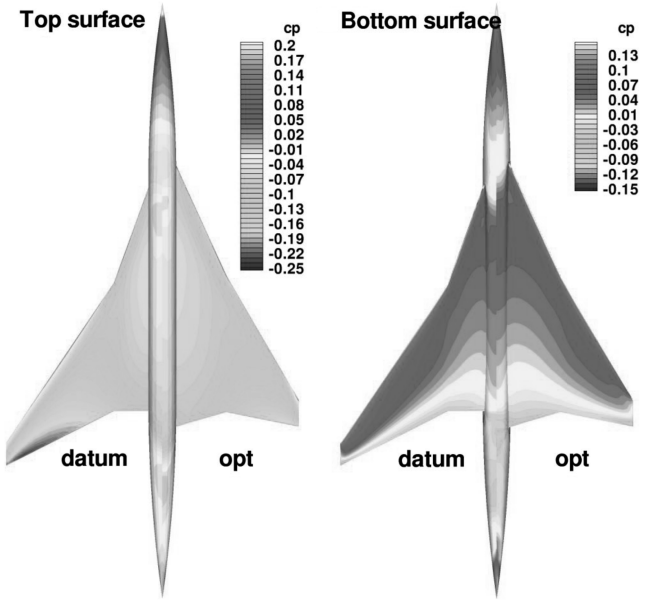

Fig. 4 Surface pressure distribution at supersonic cruise for the datum and the optimized $M = 1.6$ aircraft.

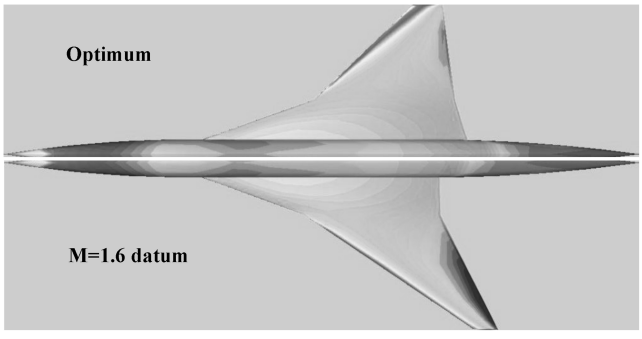

Fig. 5 Optimization of an $M = 1.6$ aircraft starting from the $M = 1.6$ datum configuration.

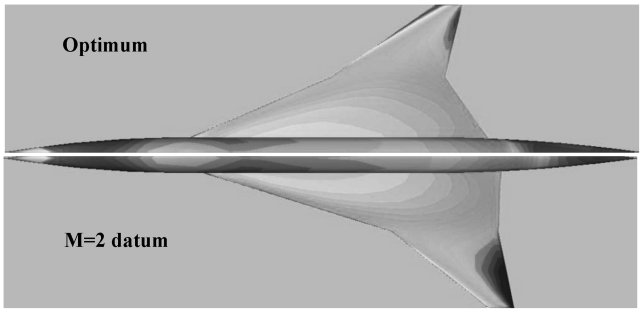

Fig. 6 Optimization of an $M = 1.6$ aircraft starting from a $M = 2$ datum configuration.

While executing the CISAP project, a large number of optimization runs have been performed using different sets of variables and starting points. These activities already helped to explore the design space, and it was felt that the design space for this specific application is relatively flat but not smooth.

To get a better understanding, some additional effort tries to find a global optimum in parallel to address the design space topology. For this, an even more intense design space exploration based on a genetic algorithm is conducted.

The full design space (15 variables) is explored by a very long optimization run using a differential evolution (DE) algorithm [13] (400 generations each having 10 individuals). The computational effort needed is characterized by the following numbers. A single MD analysis including several iterations of the CFD and FEM solvers takes about 14 min on an older PC (2800 MHz Intel processor), and typical optimizations were run for 200 to 500 optimizer steps. The long DE run (4000 steps) thus took, on a four-node PC cluster, nearly 10 days.

The DE algorithm does not converge to a distinct optimum, but indicates range peaks for very similar planforms (not shown) cruising comparable ranges ($\Delta R < 40$ n miles). It is furthermore observed that the slope of the visualized "hill" is seeded with local minima, which is visible in an approximate visualization of the multidimensional design space. All a/c traveling farther than 4900 n miles are depicted in Fig. 7 as bars over the reduced variable space. Based on the main range drivers, L/D in cruise and wing weight, the plotting plain is defined. In the present visualization, the results are clustered towards the upper right corner.

It can be concluded that different practical approaches lead to significant range increases of varying magnitude. Thus, the optimization results seem to have converged more to local maxima than to global. Nevertheless, in light of the obtained range increases, the proof of having found the global optimum, from an engineering point of view, is of second interest. The applications show, that the SubPlex optimizer is very efficient and better suited to approach a global optimum than the previous used Nelder–Mead method. This holds, even if the Nelder–Mead method is applied in a sequenced manner. Beyond this, in case only small performance improvements are obtained, a verification of the best result by an alternate optimization using another starting point is recommended.

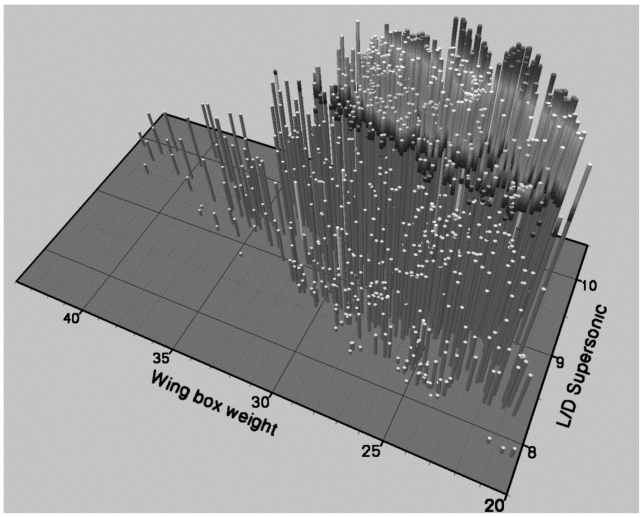

Fig. 7 Visualization of a design space approximated as range (bar length) over wing weight and supersonic L/D.

IV. Aerodynamic Off-Design Analysis of the Multiple Discipline Optimized $M = 1.6$ Configuration

Although most time of the mission is spent in supersonic cruise, the aerodynamic performances during the other flight phases also drive the mission range. Therefore, the magnitude of these values, estimated by the empirical modules while running the MDO, is addressed next. Again, DLR's high-fidelity aerodynamic tools are applied.

These tools are the two Reynolds averaged Navier–Stokes (RANS) flow solvers being available at DLR. Because of the differing geometric complexity of the configuration at the two interesting speed ranges, a clean wing at transonics and, at low speeds, a wing featuring deflected leading and trailing edges, two mesh types had to be generated used. At the transonic conditions, a structured mesh is used, and the associated flow solver is the DLR FLOWer code [9]. The low-speed configuration required an unstructured mesh and the use of the DLR Triangular Adaptive Upwind Scheme (TAU) flow solver [14].

The aerodynamic analysis of the optimized $M = 1.6$ configuration concentrates on low speed and transonic performance. For the optimized configuration (see Fig. 4) the transonic cruise performance at $M = 0.95$, $C_L = 0.2$, $Re = 685 \times 10^6$ is estimated by the empirical model to reach an L/D of 15.4.

A potential proof of the empirical model prediction is obtained by computing the viscous transonic performance for this configuration. The necessary viscous computation is performed on a structured eight-block mesh (1 million cells, boundary-layer resolution of 24 cells) at a lower Reynolds number of 22.5×10^6. Numerical difficulties were expected for the computation simulating the high flight Reynolds number. Therefore, this number was reduced to a value for which also experimental results exist, at least at low speed (although for another configuration).

The presented viscous transonic computations are performed at a constant angle of attack (AOA). Two pressure distributions at $\alpha = 4.5$ deg ($C_L = 0.18$ being slightly below the target of $C_L = 0.2$) are given on the left-hand side of Fig. 8. The transonic flow is characterized by a strong expansion near the leading edge of the wing, producing a pretty large separation mainly on the outer wing trapezium. A shock develops near the trailing edge.

On the right-hand side of Fig. 8, the computed aerodynamic performances at three AOA are plotted for two mesh densities (coarse C and medium dense M). The aerodynamic performance value estimated by the mission module is indicated in this graph by the crossing blue lines. Although a strong vortex is computed (even at $C_L < 0.2$), see the high suction peak at about $X/C = 0.1$ on the outer wing in the left-hand side graph of Fig. 8; the estimated performance on the medium dense mesh does not differ much from the "target" value predicted by the empirical model in the MDO process. Please note that, for flight conditions, the friction drag will reduce due to the increased Reynolds number and will thus further improve the aerodynamic performance.

An existing leading- and trailing-edge flap-based high-lift system for such an aircraft would obviously be used to adapt the wing to transonic cruise conditions. The appropriate deflection distribution of the leading- and trailing-edge flaps would prevent the observed strong separations and the associated drag increase. Therefore, such a wing adaptation would improve the aircraft's aerodynamic performance in transonics considerably.

It is concluded that the transonic RANS results of the current optimal aircraft configuration confirm the empirical model estimations used within the MDO process. Because no leading and trailing edge flaps adapting the wing to transonic cruise conditions

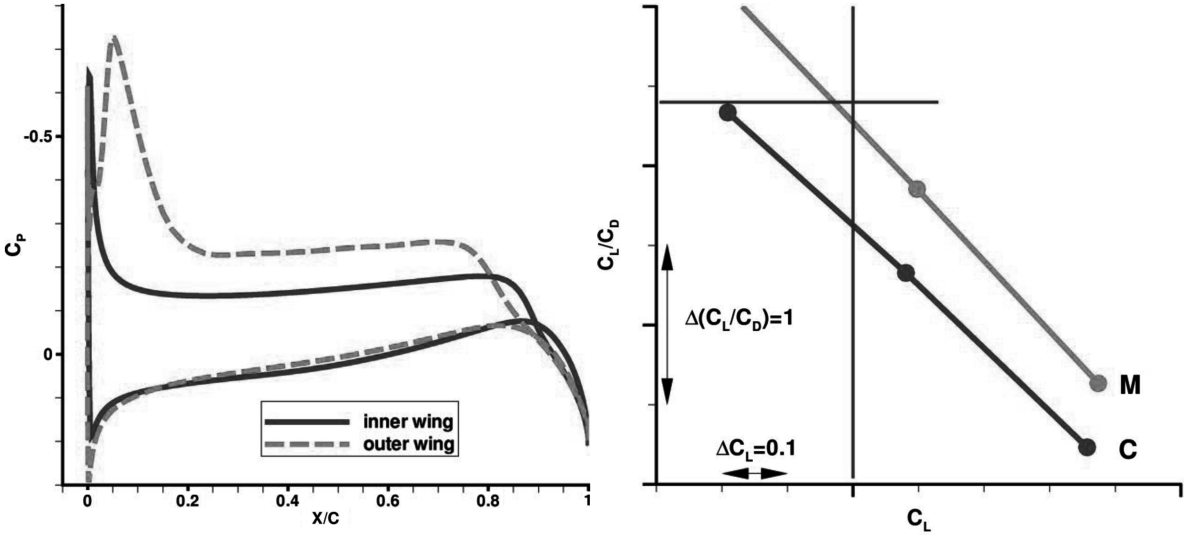

Fig. 8 Viscous transonic pressure distribution and aerodynamic performance estimation of the optimized $M = 1.6$ configuration.

have been considered yet, further potential for aerodynamic improvement is assumed.

Because the aerodynamic performance of the optimized aircraft at transonics is well predicted, it is concluded that the implemented empirical model is well tuned for the current purpose.

At low speeds, the empirical model of the MDA process assumes a highly efficient high-lift system delivering superior aerodynamic performance. These performance estimations by the empirical model are shown in Table 2 for the two most important low-speed flight conditions. The low-speed climb-out flight phase is of significant importance because of the critical noise certification for any new a/c.

To be able to judge the prediction accuracy of the empirical model, it is necessary to compare to higher-fidelity results obtained by RANS computations, as already explained. These results need to incorporate an efficient high-lift system, posing the problem to define such a high-lift system for this multiple discipline optimized configuration. Previous experience [15] ruled to check the initial low-speed flow topology (no high-lift system) first.

An initial low-speed RANS computation for the clean wing is thus conducted. The clean wing low-speed flow is characterized by a large vortex. Thus, the associated aerodynamic performance is low (L/D of 4.7) on approach. More details are reported in an earlier paper on this topic [10].

A high-lift system matching lift and angle of attack constrains ($C_L \sim 0.64$; $\alpha < 12$ deg) is designed for the clean wing. Based on experience and some test calculations, the trailing edge (TE) flaps are deflected by 15 deg. As leading edge (LE) flap deflections cause some lift loss, only a weak deflection of 10 deg is selected for the outer wing. A trapped vortex on the deflected LE flap is known to reduce drag. To trigger this on the inner wing, the LE flap is deflected by 15 deg here. The adapted unstructured mesh for the optimized $M = 1.6a/c$ (high-lift system deployed) consists of 13.3×10^6 nodes, with 20 prismatic layers resolving the boundary layer (see Fig. 9). The decided slat and flap setting is used for both low-speed flight conditions, knowing that this may represent an over-simplification.

Table 2 Low-speed aerodynamic performance empirical model estimations

	Empirical model estimations	
Low-speed condition	Approach	Climb out
Mach number	0.22	0.38
target lift	0.64	0.39
Angle of attack	≤ 12 deg	≈ 4.7 deg
L/D	≈ 5.86	≈ 12.33

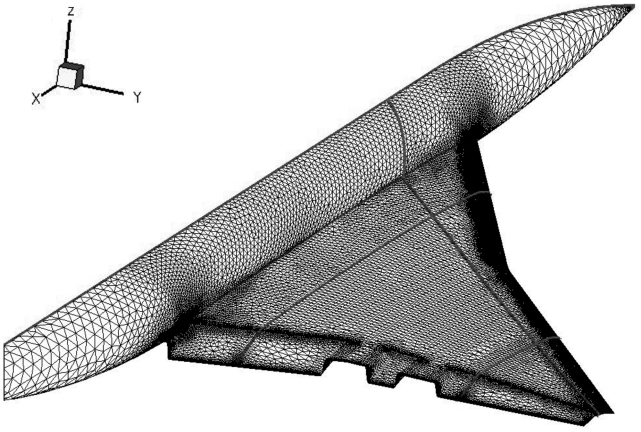

Fig. 9 Unstructured surface mesh on the CISAP optimized a/c with high-lift system deployed.

The flow is computed with the DLR TAU code [14] and is found to be mainly attached at $\alpha = 4.7$ deg (see Fig. 10, left) for the climb-out phase. The lift (climb out) is obtained within common accuracy limits [16].

The CFD estimated low-speed performances are compared for the two wings (clean and with high-lift system) to the empirical model results in Fig. 11. The lift over drag ratios are plotted against the obtained lift at low speeds. A RANS-computed large performance increase of about 35% at the climb out C_L of 0.39 is obtained through the high-lift system compared with the clean wing. Nevertheless, this performance is still lower than the value estimated by the empirical model used in the MDO process.

Some additional drag reductions, compared here with the assumed high-lift system of the multiple discipline optimized aircraft, might be obtained by relying on increased LE flap chords and by a more appropriate leading-edge flap deflection distribution for the flight's climb-out (higher deflection angles) phase. To account for the associated lift loss, the TE flaps would need higher deflections. It is believed that the TE hinge suction peaks might not reach separation onset values. Nevertheless, based on practical experience regarding the high-lift system design for such types of wings, doubt remains regarding further low-speed performance increases by an alternate high-lift system.

The solution in Fig. 10, right, is nearest to the approach lift of 0.64. A primary vortex near the leading edge is developing, and another (weak) vortex runs parallel to the fuselage. The pressure peaks at the TE flap hinges are visible. The $\alpha < 12$ deg constraint on approach is

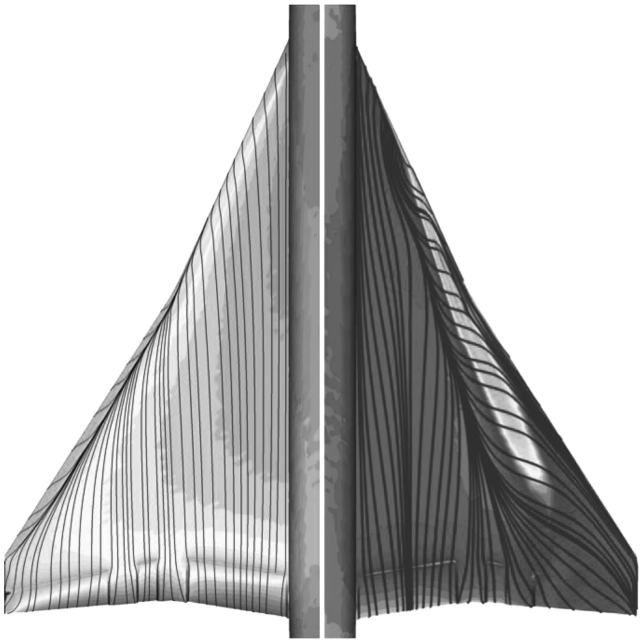

Fig. 10 Low-speed flow topologies on the optimized a/c with high-lift system: left) climb out; right) approach condition.

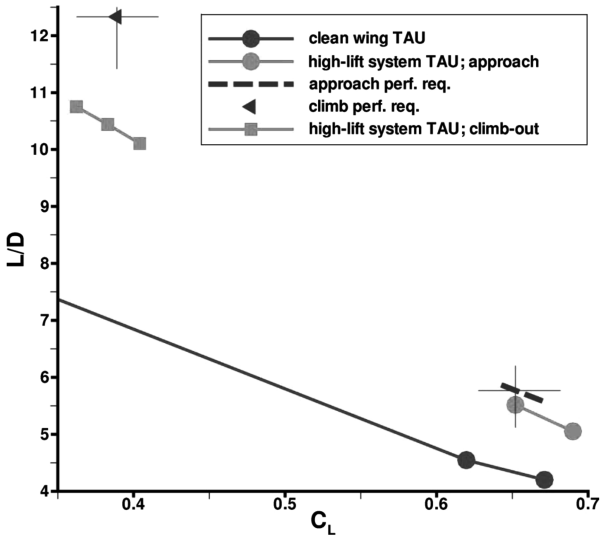

Fig. 11 Comparison of low-speed performance estimation between viscous CFD and empirical model.

met. The performance increase obtained by the high-lift system is around 28% compared with the clean wing at the high lift of $C_L = 0.65$. The approach performance (empirical model) is nearly completely (95%) met by the selected high-lift system.

The approach performance estimation by the empirical model is thus found to be very adequate. The angle-of-attack constraint is kept, and the L/D value is well met. The selected high-lift system flap setting is well balanced between the necessary lift increase (TE) and the drag reduction (LE) for the approach flight phase. But, it is concluded that the climb-out phase modeling of the empirical model within the MDO process is too optimistic and should be better adjusted. In case of further optimizations considering noise issues, the modeling of this flight phase would need further consideration because the climb-out performance determines the aircraft's altitude at the fly over noise measurement point.

V. Conclusions

Within the CISAP project, DLR developed its own multidiscipline optimization (MDO) process using high-fidelity tools modeling the supersonic cruise leg of a complete aircraft mission. This part of the aircraft mission sizes the a/c structure to hold the aerodynamic load experienced during a 2.5 g pull-up maneuver. The DLR MDO process is based upon a provided multidisciplinary analysis suite. Within this suite, the structural maneuver loads (NASTRAN FEM code) as well as the aerodynamic cruise performance (DLR flow solver FLOWer in Euler mode) are estimated based on high-fidelity tools for the cruise part of the mission.

The implemented process, therefore, combines constrained aerodynamic shape optimization with stressed structures of minimized weight plus lower fidelity formulations for other disciplines (propulsion, flight mechanics) involved and off-design aerodynamics. The MDO design objective is to maximize the cruise range starting from fixed takeoff weights.

Manual and fully automated optimization approached are applied using different sets of global design variables. The optimized configurations obtain significant range improvements in the order of 20%. This is primarily achieved because of a changed wing shape shifting the load inboards and, furthermore, allowing a straight load path resulting in lighter wing structures.

Comparing the optimization results originating from the fully automated approach to the manual approach relying on a sequence of independent optimizations using differing subsets of variables reveals the following. Both approaches predict similar range increments because of comparable weight reductions. Nevertheless, the differences in the obtained wing planforms (from differing optimization starting points) indicate that the design space is relative flat and seeded with local maxima. Beyond these indications, the whole design space has been examined with a kind of genetic algorithm confirming the previously described finding. It is concluded that from an engineering point of view, that is, looking for an efficient way to obtain performance increases, both presented optimization approaches work reliably well.

The paper's second part compares the aerodynamic predictions of the processes (lower fidelity) models at off-design conditions. For this viscous flow computations (i.e., Reynolds averaged Navier–Stokes method) at transonic and low speed, high-lift conditions are conducted on high-density meshes. The associated computational effort is much too high to incorporate these simulations in the MDO process itself. Nevertheless, these computations serve to assess both the empirical models used in the MDO process and the obtained optimal aircraft configurations.

Applying lesson learned in the European project EPISTLE, a leading- and trailing-edge-based high-lift system for the optimized aircraft is designed. High aerodynamic low-speed performance improvements (around 35%) due to the high-lift system are estimated relying on the viscous computations at climb-out conditions. Still, the performance is below the target values estimated by the empirical model. It is, therefore, concluded that this model predicts too optimistic low-speed performance values for the $M = 1.6$ optimized configuration at the climb-out flight phase.

On approach (low speed), as well as for transonic cruise conditions, the aerodynamic performance levels of the empirical model are found pretty much in line with the viscous CFD verifications.

Acknowledgments

The author would like to thank A. Ronzheimer (MegaCads support), H. von Geyr (MDO process coworker), H. von Geyr and R. Wilhelm (unstructured meshing), as well as J. Brezillon (SPP support).

References

[1] Herrmann, U., "CISAP: Cruise Speed Impact on Supersonic Aircraft Planform: a Project Overview," AIAA Paper 2004-4539, Aug. 2004.

[2] Laban, M., "Multi-Disciplinary Analysis and Optimization of Supersonic Transport Aircraft Wing Planforms," AIAA Paper 2004-4542, Aug. 2004.

[3] Laban, M., Herrmann, U., "Multi-Disciplinary Analysis and Optimisation Applied to Supersonic Aircraft; Part 1: Analysis Tools,"

AIAA Paper 2007-1857, April 2007.
[4] Herrmann, U., and Laban, M., "Multi-Disciplinary Analysis and Optimisation Applied to Supersonic Aircraft; Part 2: Analysis Tools," AIAA Paper 2007-1858, April 2007.
[5] Torenbeek, E., Jesse, E., and Laban, M., "Conceptual Design of a Mach 1.6 European Commercial Transport," AIAA Paper 2004-4541, Aug. 2004.
[6] Synaps Ingenieur-Gesellschaft mbH, SynapsPointer Pro V2.50, Synaps Ingenieur-Gesellschaft mbH, Bremen, Germany, 2002.
[7] MSC.NASTRAN 2001 Quick Reference Guide, MSC Software Corporation, Santa Ana, CA, 2002.
[8] Brodersen, O., Hepperle, M., Ronzheimer, A., Rossow, C.-C., and Schöning, B., "The Parametric Grid Generation System MegaCads," *5th International Conference on Numerical Grid Generation in Computational Field Simulation*, edited by Soni, B. K., Thompson, J. F., Häuser, J., and Eiseman, P. R., National Science Foundation, Arlington, VA, 1996, pp. 3535–3562.
[9] Kroll, N., Rossow, C.-C., Becker, K., and Thiele, F., "MEGAFLOW: A Numerical Flow Simulation System," *Aerospace Science and Technology*, Vol. 4, No. 4, 2000, pp. 223–237. doi:10.1016/S1270-9638(00)00131-0
[10] Herrmann, U., Freiherr von Geyr, H., and Werner-Westphal, Ch., "Mixed Fidelity Multi Discipline Optimization of a Supersonic Transport Aircraft," AIAA Paper 2005-534, Jan. 2005.
[11] Nelder, J. A., and Mead, R., A Simplex Method for Function Minimization, *Computational Journal*, Vol. 7, 1965, pp. 308–313.
[12] Rowan, T. H., "Functional Stability Analysis Of Numerical Algorithms," Ph.D. Thesis, Department of Computer Sciences, University of Texas at Austin Austin, TX, May 1990.
[13] Storn, R., and Price, K., "Differential Evolution: A Simple and Efficient Adaptive Scheme for Global Optimization over Continuous Spaces," International Computer Science Institute, Tech. Rept. TR-95-012, 1995.
[14] Gerhold, T., Galle, M., Friedrich, O., and Evans, J., "Calculation of Complex Three-Dimensional Configurations Employing the DLR-TAU Code," AIAA Paper 1997-167, Jan. 1997.
[15] Herrmann, U., "Current Aerodynamic High-Lift System Design Work for SSTs: A European Perspective," *4th SST-CFD Workshop*, Japanese Aerospace Exploration Agency, Tokyo, Oct. 2006, Invited Lecture No. 7.
[16] Herrmann, U., Press, A., Newbold, C., Kaurinkoski, P., Artiles, C., Muijden, J. V., and Carrieri, G. "Validation of European CFD Codes for SCT Low-Speed High-Lift Computations," AIAA Paper 2001-2405, June 2001.